Forest Ecology and Management 620 (2026) 124172

Contents lists available at ScienceDirect

Forest Ecology and Management

journal homepage: www.elsevier.com/locate/foreco

Spatial variation of snow-pressure-induced basal sweep in Japanese cedar (*Cryptomeria japonica* D. Don) plantations along a snow gradient

Kotaro Zushi *, Akio Kato [1], Hisashi Sugita

Forest Research Institute, Toyama Prefectural Agricultural, Forestry and Fisheries Research Center, 3 Yoshimine, Nakaniikawa, Toyama 930-1362, Japan

ARTICLE INFO

Keywords:
Basal sweep
Snow-pressure damage
Compositional data analysis
Random forest
Site index
Spatial modelling

ABSTRACT

In snowy regions of Japan, seedlings of Japanese cedar (*Cryptomeria japonica* D. Don), the dominant plantation species, are chronically deformed by snow-pressure loading during snow burial. The resulting basal sweep persists throughout the rotation and lowers both merchantable volume and product grade. Despite this economic significance, its broad-scale spatial variation has not been modelled. Here we develop one to predict stand-level stem-form composition from environmental drivers. We surveyed 638 plots (11.3 m radius; stand age ≥ 40 years) across 7406 ha of plantations in Toyama Prefecture, central Japan, scoring deformation as the relative abundance of four stem-form classes, from straight (c1) to severely swept (c4). Using compositional data analysis, two principal components captured 92% of among-stand variation: the first contrasted straight stems (c1) with more-swept stems (c3, c4); the second reflected mildly swept stems (c2). A random forest with four mechanistically chosen predictors — snow depth, site index, slope, and aspect — explained 45.7% of compositional variation. Snow depth dominated: the proportion of straight stems fell from 55% to 10% as mean annual maximum snow depth rose from 0.5 to 1.8 m. Site index had the opposite, monotonic effect, consistent with rapid early height growth letting seedlings outgrow the snow-burial window. Slope showed breakpoints near 15° and 32°, and aspect produced an asymmetric, insolation-driven response. Mapped regionally, predictions revealed a strong elevational contrast and east–west gradients at low elevation. This provides the first wall-to-wall prediction of snow-pressure-induced stem quality, supporting grade-aware forecasting and reforestation planning in snowy forests.

1. Introduction

Snow is, alongside wind, a primary abiotic disturbance agent in boreal, oceanic temperate and montane forests (Nykänen et al., 1997; Peltola et al., 2000). Approximately 4 million m^3 of timber are lost annually to snow damage within the European Union (Nykänen et al., 1997), and this economic impact is comparable or greater when the snowy and mountainous forests of North America and East Asia are taken into account. Recent events underscore the scale of these losses: a single severe snow-damage episode in Finland in the winter of 2017–2018 caused an estimated 7–10 million euros in losses to forest owners (Tomppo et al., 2019). How the frequency and severity of snow damage will change under altered snowfall regimes is a major question in adaptive forest management. In northern Europe, the climatically suitable zone for snow and ice damage is projected to shift northward (Suvanto et al., 2021; Venäläinen et al., 2020), and in central Europe, shorter rotations have been proposed as part of broader strategies to mitigate snow and wind risk (Zimovà et al., 2020).

Snow damage to trees is conventionally separated into two mechanistically distinct types according to the developmental stage of the trees affected (Noomote, 1989; Shidei, 1954; Taira, 1987). *Crown snow damage* occurs when accumulated snow on the canopy exceeds the bending or anchorage capacity of the stem and roots, producing stem breakage, crown breakage or uprooting. It affects sapling and pole-stage to mature stands and is strongly modulated by tree- and stand-level structural attributes such as stem taper, crown form and stocking (Päätalo, 2000; Peltola and Kellomäki, 1993; Peltola et al., 1997; Petty and Worrell, 1981). For Scots pine (*Pinus sylvestris*) and Norway spruce (*Picea abies*) plantations in northern and central Europe, mechanistic models of crown snow and ice damage (Gardiner et al., 2000; Peltola et al., 1999) have been integrated into stand-level management guidelines. *Snow-pressure damage*, in contrast, occurs when seedlings and young saplings become buried by snow and are continuously subjected to creep and glide forces during the snow-buried phase, producing characteristic basal sweep of the stem (Shidei, 1954; Taira, 1982, 1985). Whereas crown snow damage is acute and event-driven,

* Corresponding author.
E-mail address: kotaro.zushi@pref.toyama.lg.jp (K. Zushi).

[1] Retired.

https://doi.org/10.1016/j.foreco.2026.124172
Received 8 June 2026; Received in revised form 21 July 2026; Accepted 24 July 2026
0378-1127/© 2026 Elsevier B.V. All rights reserved, including those for text and data mining, AI training, and similar technologies.

affecting a subset of trees in a stand, snow-pressure damage is chronic and cumulative, acting on virtually all trees in a stand during their juvenile phase across consecutive winters and producing a persistent reduction in merchantable volume and lumber grade (Hada, 1960; Kataoka and Sato, 1959; Zushi and Kato, 2015). This study addresses the latter.

Snow-induced stem deformation has been reported from snowy and mountainous forests worldwide. In the subalpine zone of the European Alps, snow creep and glide on steep slopes exert continuous downslope shear on young *Pinus cembra* and *Larix decidua*, causing uprooting and stem deformation (Frutiger and Kuster, 1967; Höller et al., 2009; In der Gand, 1968; Leitinger et al., 2008). In the deep-snow belts of the Rocky Mountains in North America, similar prostration and stem deformation of young conifers have been documented (Leaphart et al., 1972; Schmidt and Schmidt, 1979). Although the climatic and topographic settings differ, these phenomena share a common mechanism: juvenile trees are subjected to repeated snow loading during the snow-buried phase, and the resulting deformations accumulate as the stem matures.

The Sea of Japan coast of the Japanese archipelago is one of the snowiest regions in the world. When the cold Siberian monsoon passes over the Sea of Japan, it absorbs substantial moisture from the Tsushima Warm Current; the resulting moist air masses are forced to rise orographically upon reaching the mountain ranges of the archipelago, producing an exceptionally deep and persistent snowpack along the Sea of Japan coast of Honshu. In this climate, other major plantation conifers such as Japanese cypress (*Chamaecyparis obtusa*) and Japanese larch (*Larix kaempferi*) exhibit low tolerance to snow-pressure damage (Kono, 1934; Taira, 1987), and Japanese cedar (*Cryptomeria japonica* D. Don) has therefore become the dominant plantation species. Japanese cedar itself, however, is not exempt from juvenile snow prostration, and basal sweep is a ubiquitous feature of plantations in the region (Hada, 1960; Kataoka and Sato, 1959).

Snow-pressure damage in juvenile Japanese cedar plantations is initiated when early-winter snow accumulation on the crown tilts the stem, which is subsequently prostrated from the base by the creep and glide forces of the encroaching snowpack (Shidei, 1954; Taira, 1982). The deformation near the stem base (basal sweep) accumulates through root-system damage during prostration and through compression-wood formation, which together drive stem righting after snowmelt and fix the residual bend in place (Taira, 1991). The severity of damage at a given site is governed, to first order, by two factors: the depth of the snowpack and the height growth rate of saplings during the snow-burial window (Noomote, 1992). Trees are at risk of being buried until they reach approximately 2.0–2.5 times the snow depth, and the loading is maximised when the tree height is comparable to the snow depth (Shidei, 1954). Faster height growth therefore shortens the snow-burial window and reduces cumulative deformation. Because height growth rate is governed by site productivity, sites with higher site index should yield trees with lower basal sweep, all else being equal. Topography modulates these effects: steeper slopes increase the prostration angle of buried stems (Kataoka and Sato, 1959; Kono, 1934; Taira, 1987; Tsukahara et al., 1975), while aspect controls snow persistence through insolation, with north-facing slopes retaining snow longer and accumulating greater cumulative load (Kono, 1934).

Although basal sweep is an individual-tree phenomenon, it affects virtually all trees in a stand and therefore manifests as a stand-level reduction in timber quality. Quantifying its broad-scale spatial variation has several practical implications. First, basal sweep directly determines merchantable volume and product-grade-specific volume (Zushi and Kato, 2015; Zushi et al., 2017); its spatial distribution is thus a prerequisite for regional estimation of timber supply by product grade. Second, snow-pressure mitigation relies heavily on "snow lifting" (*yuki-okoshi*), the manual righting of leaning saplings, which effectively reduces eventual deformation. Because this practice accounts for a large share of operating cost in heavy-snow plantations (Noomote, 1984; Zushi, 2024), spatial identification of high- and low-risk areas supports cost-effective allocation of silvicultural effort and selection of reforestation sites. Third, expressing basal sweep as a function of environmental drivers provides a basis for projecting how future changes in the snowfall regime may alter stem quality, and for designing long-term adaptation strategies including species and provenance selection. Despite these motivations, no spatial model treating basal sweep as the response variable has been reported, in marked contrast to the well-developed spatial risk models for crown snow and ice damage in Europe (Päätalo, 2000; Suvanto et al., 2021).

A practical broad-scale survey of basal sweep requires an indicator that (i) can be applied rapidly across many stands, and (ii) preserves the within-stand distribution of deformation severity. Individual-tree metrics such as the rise of the arc or stem deviation (Hada, 1960; Kataoka and Sato, 1959; Taira, 1982; Tsukahara et al., 1975) satisfy neither criterion: they are labour-intensive and, when aggregated to stand means, discard information on the within-stand distribution of deformation severity. In contrast, the stem-form-class system (Imanaga et al., 1979; Zushi and Kato, 2015), in which each tree is visually classified into one of five ordinal severity grades, is operationally simple and rapid and yields, at the stand level, a compositional vector (relative frequency of each class) that retains the multidimensional structure of within-stand variation.

We surveyed 638 plots across Japanese cedar plantations in Toyama Prefecture, central Japan, and analysed stand-level stem-form-class composition as the response variable. Our objectives were (1) to characterise the structure of among-stand variation in stem-form-class composition and the dominant axes along which stands differ; (2) to quantify the contribution of four mechanistically derived environmental covariates — annual maximum snow depth, site index, slope gradient and northness — to that variation using random forest models, with particular attention to threshold and saturation responses; and (3) to apply the fitted model across the study area to clarify the spatial distribution of stem quality by region and elevation belt. The work transposes the spatial-modelling tradition developed in Europe for crown-type, event-driven snow damage onto the chronic, snow-pressure-driven deformation that characterises oceanic heavy-snow regions, expressing the response at the level of stand compositional structure and deriving its broad-scale variation from a parsimonious set of environmental drivers grounded in the damage-formation mechanism.

2. Materials and methods

2.1. Study area

The study was conducted in Japanese cedar plantations managed by the Toyama Prefectural Agriculture, Forestry and Fisheries Public Corporation (hereafter TAFPC) in Toyama Prefecture, central Honshu, Japan (36°24′40″–36°58′8″N, 136°47′26″–137°38′2″ E; elevation 7–1223 m; Fig. 1). Plantation establishment began in 1966 and peaked in the 1970s, when 300–400 ha were planted annually; planting continued at a declining rate until 2004. As of 2023, TAFPC managed 7406 ha of plantations across 346 management units, equivalent to approximately 15% of the privately owned planted forest in the prefecture (Zushi, 2024).

Plantations were established at a standard initial density of 2500 trees ha^{-1}. Three local varieties of Japanese cedar were planted: Tateyama-sugi, Kawaidani-sugi and Boka-sugi. Tateyama-sugi was propagated from seed, whereas Kawaidani-sugi and Boka-sugi were propagated from cuttings. Silvicultural operations, including weeding, snow lifting and pruning, were conducted as required, following TAFPC's standard operating procedures. Under these procedures, stands were scheduled to be thinned three times between the completion of weeding and approximately 40 years of age; however, management records indicate substantial variation in thinning history, ranging from stands that had never been thinned to those that had undergone four or more thinning operations.

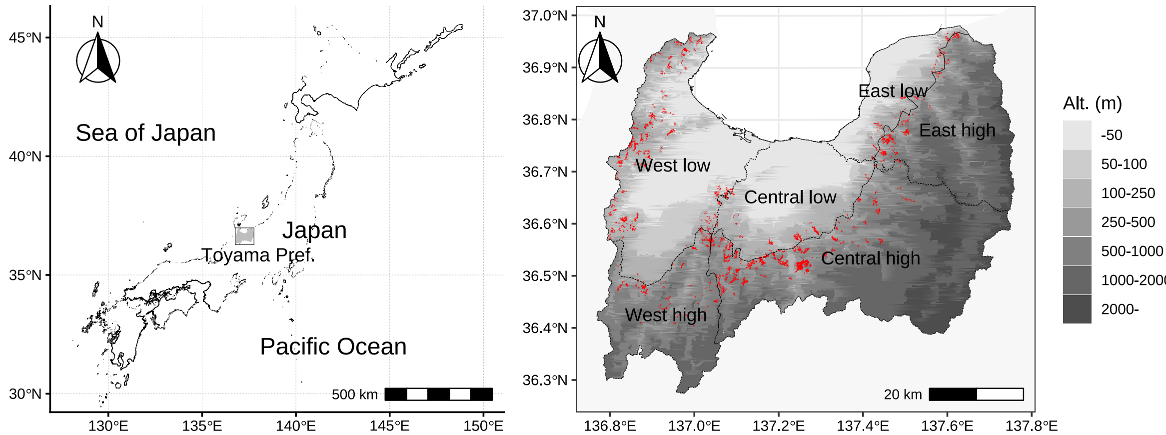

Fig. 1. Location of Toyama Prefecture within Japan (left) and spatial distribution of the Toyama Prefectural Agriculture, Forestry and Fisheries Public Corporation (TAFPC) plantations (shown in red) within the prefecture (right).

Table 1
Climate normals (1981–2010) of the surveyed plots managed by the public corporation.

Variable	Median (Min–Max)
Mean annual maximum snow depth (m)	1.66 (0.15–4.07)
Annual precipitation (mm)	2578 (2145–3277)
Mean annual temperature (°C)	12.0 (7.9–14.0)

Table 2
Stand attributes of the survey plots (N = 638).

Variable	Median (Min–Max)
Stand age (years)	44 (40–55)
Mean DBH (cm)	29.1 (16.6–46.6)
Mean tree height (m)	18.9 (9.1–28.1)
Stand density (ha^{-1})	675 (225–1719)
Stand volume (m^3 ha^{-1})	424 (82–1129)
Mean stem volume (m^3)	0.62 (0.12–1.96)

The mean and range of the climate normals (1981–2010) for the studied plantations, including mean annual temperature, annual precipitation, and mean annual maximum snow depth, are summarised in Table 1. These data were derived from a 1-km gridded national climate normal dataset (Ministry of Land, Infrastructure, Transport and Tourism (MLIT), 2026), with snow depth corrected using monthly mean temperature and monthly precipitation following Aiura et al. (2018). The dataset provides nationwide climate normals for the 30-year baseline period from 1981 to 2010. The region lies on the Sea of Japan side of central Honshu and has a humid temperate climate with cold, snowy winters. Climate is strongly conditioned by the Hida Mountains (peaks exceeding 3000 m) to the southeast: cold north-westerly monsoon air, saturated as it crosses the Sea of Japan, is forced to ascend over this barrier, producing intense orographic snowfall that accumulates as a deep, long-lasting snowpack in the mountainous interior.

2.2. Forest inventory and assessment of stem form

A total of 638 circular plots (r = 11.3 m; plot area 400 m^2) were established in plantations of age ≥40 years (the planned rotation age) between 2015 and 2017. All living trees in each plot were measured for diameter at breast height (DBH, 1.3 m above ground) and total height, and plot positions were recorded with a handheld GPS receiver. Trees with height less than 60% of the plot mean height were classified as subordinate and excluded from analysis, leaving 17 954 trees across the 638 plots for stem-form assessment. Plot-level stand attributes are summarised in Table 2.

Stem form was assessed visually using the stem-form-class system of Imanaga et al. (1979) and Zushi and Kato (2015), which evaluates stem deformation via visual observation and classifies it into five grades from Class 1 to Class 5 (Fig. 2). Class 1 (c1) comprised straight stems with no detectable basal sweep, or stems with sweep confined to below 0.5 m above ground. Class 2 (c2) comprised stems with sweep extending above 0.5 m but resolving below breast height (1.3 m). Class 3 (c3) comprised stems with sweep extending above breast height but resolving below 4 m. Class 4 (c4) comprised stems with sweep extending above 4 m or affecting essentially the entire stem. Class 5 (c5) comprised severely deformed or broken stems. Because c5 accounted for only 0.6% of all trees in the dataset, c4 and c5 were merged for analysis and are hereafter referred to collectively as c4.

2.3. Environmental covariates

As argued in the Introduction, the severity of snow-pressure damage is, to first order, controlled by snowpack depth and by the juvenile height growth rate, with slope gradient and aspect acting as secondary modulators. We therefore selected four environmental covariates as predictors: mean annual maximum snow depth (a proxy for snow loading), site index (a proxy for height growth rate), slope gradient and slope aspect.

Plot-level mean annual maximum snow depth was estimated from gridded climate normals (Ministry of Land, Infrastructure, Transport and Tourism (MLIT), 2026) using the empirical equation of Aiura et al. (2018):

$$S_p = -7.819 - 41.14\,\bar{T}_{\text{Nov-Feb}} + 0.66537\,P_{\text{Jan+Feb}}, \tag{1}$$

where S_p (cm) is the plot mean annual maximum snow depth, $\bar{T}_{\text{Nov-Feb}}$ (°C) is the mean air temperature for November–February, and $P_{\text{Jan+Feb}}$ (mm) is the cumulative precipitation for January–February. Monthly mean temperatures at each plot were lapse-rate corrected from the gridded values:

$$T_p = T_m + \gamma\,(Z_p - Z_m), \tag{2}$$

where T_p is the plot monthly mean temperature (°C), T_m the gridded monthly mean temperature (°C), γ the lapse rate (−0.0065 °C m^{-1}), Z_p the plot elevation (m), and Z_m the elevation of the grid cell containing the plot.

Site index was computed as the predicted mean tree height at the reference age of 40 years, obtained by fitting the Mitscherlich growth function calibrated for Japanese cedar plantations in the study region (Kato and Tanaka, 2009) to the observed plot mean tree height. Note that plot mean tree height was calculated after excluding subdominant trees (height < 60% of the plot mean) as described in Section 2.2. The growth function is expressed as:

$$H(t) = M_H \left(1 - L_H \exp(-k_H t)\right), \quad (3)$$

where $H(t)$ is the mean tree height (m) at stand age t (yr), and $L_H = 1.10$ and $k_H = 0.025$ are species-specific constants (Kato and Tanaka, 2009). M_H, the asymptotic height parameter that varies with site quality, was solved for each plot by substituting the observed mean tree height and stand age into Eq. (3).

Slope gradient and aspect were derived from a digital elevation model (DEM) using the Compound Basic Terrain Analysis tool of SAGA GIS (SAGA GIS Development Team, 2020). Aspect was transformed to northness:

$$N = \cos(\theta_{\text{aspect}}), \quad (4)$$

where N is northness and θ_{aspect} is aspect in radians. The DEM was a 10-m resampled version of a 0.5-m grid product derived from airborne LiDAR surveys conducted between 2018 and 2021 (Asia Air Survey Co., Ltd., Tokyo, Japan). Per-plot values of slope gradient and northness were averaged over all DEM cells falling within the 11.3-m plot radius (400 m^2). Plot-level summaries of all environmental covariates are given in Table 3.

2.4. Statistical analysis

Because stem-form-class abundance is count compositional data — the per-plot abundances sum to a constant (the total number of trees sampled), and what is biologically meaningful is the relative frequency of each class — we adopted the compositional data analysis framework of Aitchison (1982), which is built on Aitchison geometry and avoids the spurious correlations that arise when standard multivariate methods are applied to closed data. Zero counts (a class not observed in a given plot) were imputed using a Bayesian-multinomial count-zero multiplicative replacement (Martín-Fernández et al., 2003), which preserves the closure of the composition while assigning a small pseudo-probability to unobserved classes.

To characterise the relative variability of each class and the proportionality between pairs of classes, we computed the log-ratio variance matrix. To visualise the overall multivariate structure, we applied the centred log-ratio (*clr*) transformation followed by principal component analysis (PCA). For a composition $\mathbf{x} = (x_1, \ldots, x_D)$ with D parts, the *clr* transform of part i is

$$clr(x_i) = \ln \frac{x_i}{g(\mathbf{x})}, \quad (5)$$

where $g(\mathbf{x})$ is the geometric mean of all parts.

For predictive modelling of the compositional response, we used the isometric log-ratio (*ilr*) transform rather than *clr*. The *clr* coordinates sum to zero by construction, which introduces structural collinearity and biases variable importance measures; *ilr* produces an orthonormal coordinate system in $D-1$ Euclidean dimensions, suitable for use as a response in machine-learning algorithms (Egozcue et al., 2003). For each *ilr* coordinate:

$$z_i = \sqrt{\frac{r_i s_i}{r_i + s_i}} \ln \frac{g(\mathbf{x}_i^+)}{g(\mathbf{x}_i^-)}, \quad i = 1, \ldots, D-1, \quad (6)$$

where r_i and s_i are the number of parts in the positive and negative groups of the ith sequential binary partition and $g(\mathbf{x}_i^+)$ and $g(\mathbf{x}_i^-)$ are the corresponding geometric means. With four classes (c1–c4), the *ilr* transform yields three coordinates (z_1–z_3). We used the default orthonormal basis, whose sequential binary partition separates the classes in order of increasing deformation severity (z_1: c1 vs. c2; z_2: {c1, c2} vs. c3; z_3: {c1, c2, c3} vs. c4); the explicit coordinate definitions and sign matrix

Table 3
Environmental covariates extracted at the survey plots ($N = 638$).

Variable	Median (Min–Max)
Mean annual maximum snow depth (m)	1.67 (0.15–3.69)
Site index (H40, m)	17.64 (8.16–25.78)
Slope gradient (degrees)	23.5 (1.1–49.8)
Northness	0.10 (−0.99–1.00)

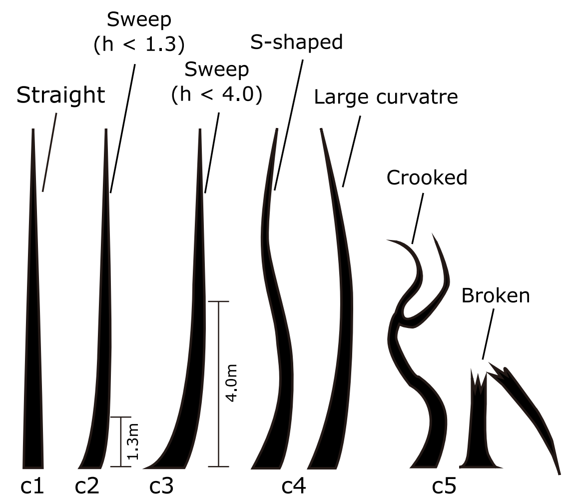

Fig. 2. Schematic illustration of the stem-form-class system used in this study. Class c1: straight or basal sweep confined to below 0.5 m; c2: sweep resolving between 0.5 m and breast height; c3: sweep resolving between breast height and 4 m; c4: sweep extending above 4 m or affecting the entire stem (the original c5 — severely deformed or broken — is merged into c4).

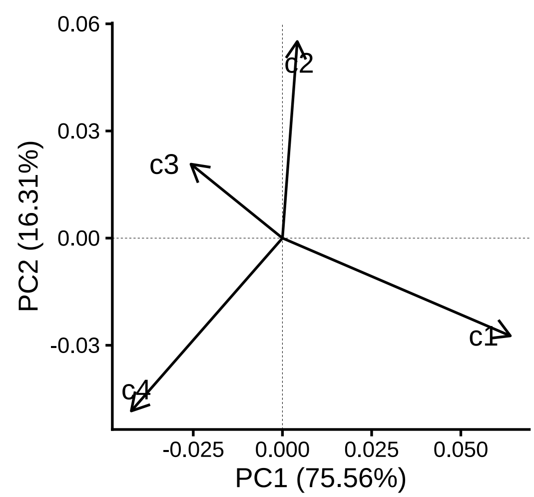

Fig. 3. Biplot of principal component analysis based on the centred log-ratio (*clr*) transform of stem-form-class composition. PC1 (75.6%) contrasts c1 with c3 and c4; PC2 (16.3%) is dominated by c2.

Table 4
Log-ratio variance matrix of the stem-form-class composition (c1: straight; c4: severely swept).

	c1	c2	c3	c4
c1	–	3.14	5.20	6.81
c2	3.14	–	1.38	2.66
c3	5.20	1.38	–	1.28
c4	6.81	2.66	1.28	–

Table 5
Class-specific predictive accuracy of the random forest model on the held-out test set ($n = 64$).

Stem-form class	R^2	RMSE
c1 (straight)	0.619	0.184
c2 (slightly swept)	0.225	0.148
c3 (moderately swept)	0.453	0.132
c4 (severely swept)	0.316	0.147

RMSE, root mean squared error.

are given in Supplementary Section S1. Predicted values in *ilr* space were back-transformed to the original simplex (composition summing to 1) by the inverse *ilr* transform.

The dataset was randomly split into a training set (90%) and a held-out test set (10%). Predictor variables were standardised (mean 0, SD 1) using parameters estimated from the training set; the same transformation was applied to the test set. Three random forest regressions, one for each *ilr* coordinate, were fitted on the training set. Hyperparameters (number of trees and number of variables tried at each split, `mtry`) were tuned by 10-fold cross-validation combined with a random grid search of 50 candidate configurations, with root mean squared error (RMSE) as the selection criterion; the search ranges, the selected values and the remaining settings are reported in Supplementary Section S3. Model accuracy was evaluated on the held-out test set as the proportion of total compositional (Aitchison) variance explained across the three *ilr* coordinates jointly (R^2_A). After back-transformation to the simplex, a class-specific coefficient of determination, computed as the squared correlation between observed and predicted proportions, was also obtained for each of the four classes. Both metrics are defined in Supplementary Section S2.

Variable importance in the random forest was assessed by permutation-based importance (Biecek, 2018). The marginal effect of each predictor was visualised using partial dependence plots (PDP) (Biecek and Baniecki, 2023). PDPs were computed on the *ilr* coordinates and then back-transformed to the simplex so that effects are interpretable as changes in class proportions.

The fitted model was applied to the full population of TAFPC's plantations. Stand polygons were tessellated into 20 m × 20 m grid cells; environmental covariates were extracted for each cell, and the model was applied to predict stem-form-class composition. The mean tree height required to compute the site index was obtained from the Japanese cedar canopy height data derived from the airborne LiDAR surveys conducted between 2018 and 2021 by Asia Air Survey Co., Ltd. (Tokyo, Japan). To summarise the spatial pattern, TAFPC's plantations were divided into eastern, central and western districts (along the jurisdictional area of TAFPC) and into low- (<350 m) and high-elevation (≥350 m) belts, yielding six sub-regions (Fig. 1).

To assess whether stand management or planting stock could confound the estimated environmental effects, we conducted sensitivity analyses in which thinning frequency (the number of thinning operations per stand) and cultivar were each added as a fifth predictor and the resulting models compared with the four-covariate model (Supplementary Section S4).

All analyses were carried out in R (R Core Team, 2024) using the packages `compositions` (van den Boogaart et al., 2025), `zCompositions` (Martín-Fernández et al., 2003), `ranger` (Wright and Ziegler, 2017), `tidymodels` (Kuhn and Wickham, 2020), `DALEX` (Biecek, 2018) and `ingredients` (Biecek and Baniecki, 2023).

3. Results

3.1. Stem-form-class composition and its variability among stands

Of 17954 trees surveyed across the 638 plots, 27.0%, 29.3%, 26.4% and 17.3% were assigned to classes c1, c2, c3 and c4, respectively. The mean composition across plots was c2 36.2%, c3 30.5%, c1 19.1% and c4 14.2%, indicating that intermediate-deformation classes dominated at the stand level even though the four classes had broadly similar overall frequencies when pooled over all trees.

The log-ratio variance matrix (Table 4) and the *clr*-based PCA biplot (Fig. 3) revealed a strongly structured pattern of among-stand variation. The smallest log-ratio variances were between c3 and c4 (1.28) and between c2 and c3 (1.38), indicating that the relative abundance of these adjacent classes was approximately conserved among stands. The largest variances involved c1: c1 vs. c4 (6.81) and c1 vs. c3 (5.20), showing that the abundance of the straight-stem class varied substantially among stands relative to the deformed classes. PCA confirmed this structure: PC1 explained 75.6% and PC2 16.3% of the total compositional variance (cumulative 91.9%). The c1 loading vector was the longest and was directed opposite to the c3 and c4 vectors along PC1, indicating a strong inverse relationship between the abundance of straight stems and that of moderately and severely swept stems. The c2 vector loaded most strongly on PC2, indicating that c2 varied independently of the c1 vs. c3/c4 contrast.

3.2. Stem-form-class composition by tree size

Class composition shifted progressively with increasing DBH and tree height (Fig. 4). In the smallest DBH class (<20 cm), c3 and c4 together accounted for more than 60% of stems, whereas in the largest class (≥45 cm) their combined share fell below 10%; c4 in particular declined from above 30% to below 5%. Conversely, c1 increased from below 10% in the smallest DBH class to approximately 65% in the largest. The same pattern was observed across tree-height classes: c1 dominated stems above 24 m in height (~60%) whereas c3 and c4 dominated stems below 14 m. The abundance of c2, by contrast, remained between 20% and 30% across all size classes, with no systematic trend. This stability of c2 along the size axis is consistent with its independent loading on PC2 (Fig. 3).

3.3. Model performance

Across all three *ilr* coordinates, the random forest model explained 45.7% of the total compositional (Aitchison) variance on the held-out test set ($R^2_A = 0.457$). Class-specific accuracy after back-transformation to the simplex (Table 5), computed as the squared correlation between observed and predicted proportions, was highest for c1 ($R^2 = 0.619$), intermediate for c3 ($R^2 = 0.453$) and c4 ($R^2 = 0.316$), and lowest for c2 ($R^2 = 0.225$).

3.4. Variable importance and partial effects

In all three *ilr*-coordinate models, mean annual maximum snow depth showed the highest variable importance, substantially exceeding that of the other predictors, and site index ranked second (Fig. 5). Slope gradient and northness ranked third and fourth, with their relative order varying among coordinates.

Partial dependence plots (Fig. 6) revealed the form of each marginal effect after back-transformation to the simplex.

Snow depth (Fig. 6A). The abundance of c1 declined sharply with increasing snow depth, from approximately 55% at 0.5 m to approximately 10% at 1.8 m, saturating near 5% above 2.5 m, while c3 and c4 increased monotonically to approximately 50% and 32% at 3 m. The response of c2 was unimodal, peaking at approximately 45% near 1.0–1.5 m.

Site index (Fig. 6B). Class abundances responded to site index in a pattern that mirrored the snow-depth response but in the opposite direction: c1 increased monotonically from approximately 8% at SI 8 to approximately 48% at SI 25, whereas c4 decreased from approximately 30% and saturated near 8% above SI 20. Overall, as site index increased, the dominant class shifted progressively from c4 through c3 and c2 to c1.

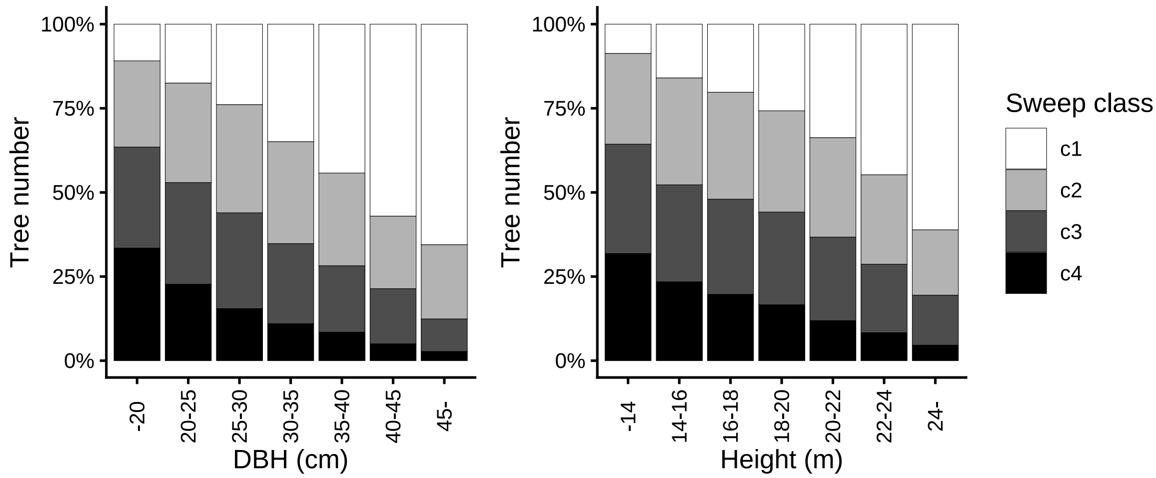

Fig. 4. Stem-form-class composition by DBH class (left) and by tree-height class (right).

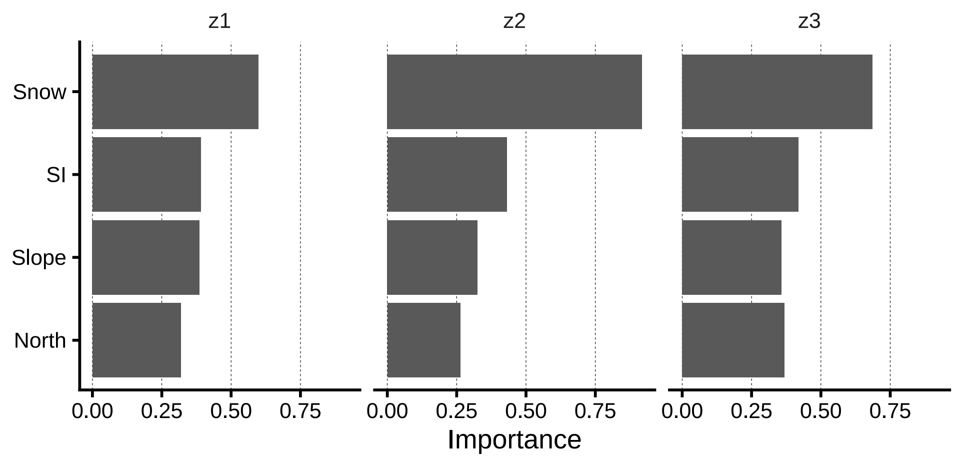

Fig. 5. Permutation-based variable importance for the random forest models of the three *ilr* coordinates (z_1–z_3). Each coordinate contrasts stem-form classes according to the sequential binary partition (z_1: c1 vs. c2; z_2: c1, c2 vs. c3; z_3: c1, c2, c3 vs. c4; see Section 2.4 and Supplementary Table S1). Abbreviations: Snow, mean annual maximum snow depth; SI, site index; Slope, slope gradient; North, northness.

Slope gradient (Fig. 6C). The slope-gradient response was non-linear and exhibited two breakpoints near 15° and 32°. The abundance of c1 was approximately constant at ~30% below 15°, declined steeply between 15° and 32°, and saturated near 13% above 32°. Above 32°, c2 rose sharply to ~43% while c4, which remained low (10%–16%) throughout, declined after peaking weakly between the two breakpoints.

Northness (Fig. 6D). The abundance of c1 was approximately twice as high on south-facing slopes (~30% at $N = -1$) as on north-facing slopes (~16% at $N = +1$), and c4 showed the opposite pattern (~9% to ~16%). The abundance of c2 was essentially insensitive to aspect (~36% across the range).

3.5. Spatial application to TAFPC's plantations

Application of the fitted model to all 20 m × 20 m cells within TAFPC's plantations produced a wall-to-wall prediction of stem-form-class composition (Fig. 7). Composition differed strongly between elevation belts: at low elevation (<350 m), c1 and c2 together accounted for approximately 60% of stems in all three districts, whereas at high elevation (≥350 m), c3 and c4 together accounted for approximately 60%. Within the low-elevation belt, the abundance of c1 declined from west to east (~38%, ~22% and ~15% in the western, central and eastern districts, respectively), whereas at high elevation it was below 10% in all three districts with no clear east–west gradient. The abundance of c4 was approximately 10% across the low-elevation belt but reached approximately 20% at high elevation, peaking at ~25% in the western high-elevation sub-region. The abundance of c2 remained close to 30% across all six sub-regions, varying less than any other class.

Combined with stand area, these patterns showed that the western low-elevation belt — an area of relatively large plantation extent — was both the largest contiguous area of high-quality (c1-rich) stands in the prefecture and the area where c3 and c4 combined were below 30%. Conversely, the central high-elevation belt, which contains the largest absolute plantation area in the prefecture, had c3 and c4 combined exceeding 55%, identifying it as the area where reduced stem quality was most widespread.

4. Discussion

4.1. Compositional structure and methodological contribution

We characterised the broad-scale spatial variation of snow-pressure-induced basal sweep in Japanese cedar plantations through the compositional structure of stem-form classes at the stand level. The PCA biplot and log-ratio variance matrix showed that compositional variation was dominated by a single inverse axis contrasting c1 with c3 and c4 (PC1, 75.6% of the variance), accompanied by an independent axis dominated by c2 (PC2, 16.3%). This two-dimensional structure summarises

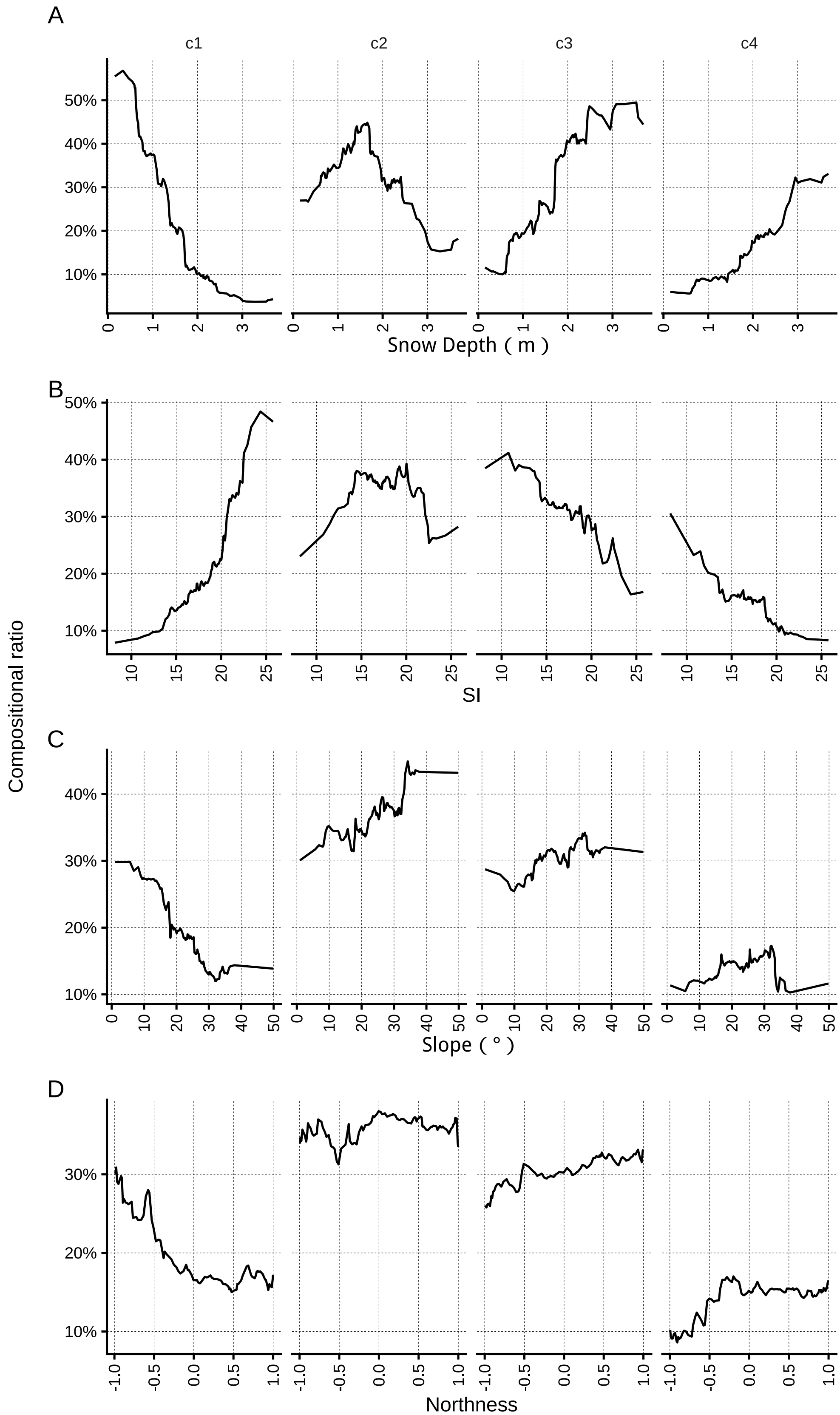

Fig. 6. Partial dependence plots showing the marginal effect of each environmental covariate on stem-form-class composition, computed on the *ilr* coordinates and back-transformed to the simplex. (A) Mean annual maximum snow depth, (B) site index, (C) slope gradient, (D) northness.

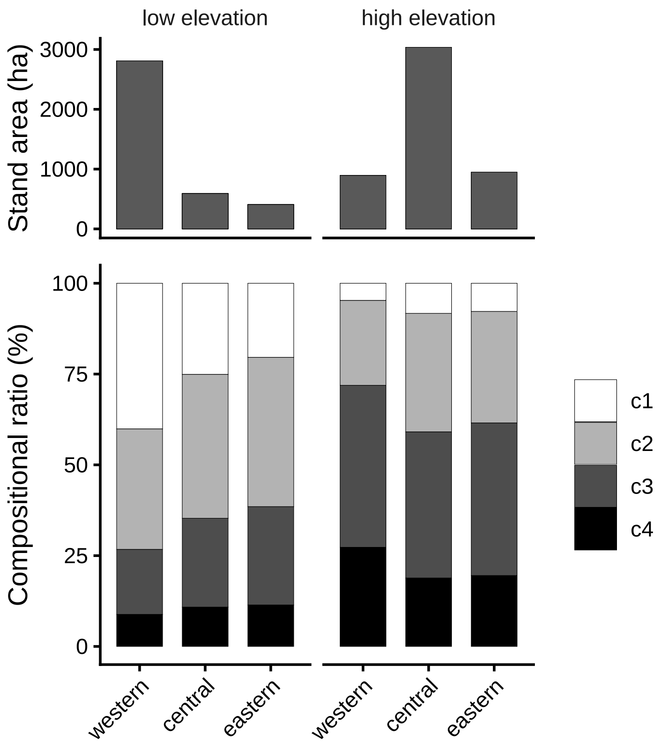

Fig. 7. Predicted stem-form-class composition of the Toyama Prefectural Agriculture, Forestry and Fisheries Public Corporation (TAFPC) plantations, summarised by district (eastern, central, western) and elevation belt (low, <350 m; high, ≥350 m). Bar widths reflect the total plantation area in each subregion.

the among-stand variation in stem quality across nearly the full range of snow and productivity conditions encountered in the region.

Earlier quantitative work on basal sweep relied on individual-tree metrics. Hada (1960) and Kataoka and Sato (1959) partitioned individual stems into swept and straight segments based on the rise of the arc, and used the basal sweep ratio — defined as the volumetric ratio of swept segments to the total stand volume — as an indicator; Kataoka and Sato (1959) further demonstrated that this ratio is closely related to annual maximum snow depth and slope gradient. Tsukahara et al. (1975) and Taira (1982, 1985) used the stem deviation as a continuous measure of basal sweep, and clarified the mechanism of sweep formation (Taira, 1991), its relation to snow depth and slope (Yano, 1987), root damage (Sudo et al., 1971), cultivar differences (Taira, 1979, 1984) and silvicultural treatment effects (Taira, 1985). These individual-tree metrics have made important contributions, but for broad-scale spatial assessment they have two limitations: they are labour-intensive to measure across many stands, and aggregating them to a stand mean discards information on the within-stand distribution of deformation severity. The stem-form-class composition adopted here avoids both limitations. Notably, our PCA showed that c2 loaded on PC2 independently of the c1 vs. c3/c4 axis, and the PDP for snow depth showed that c2 had a unimodal response distinct from the monotonic responses of the other classes. Such second-axis behaviour would be invisible to any single-valued, mean-based metric.

The earlier work cited above also considered factors other than the environment, notably cultivar and silvicultural treatment. We therefore examined both as additional predictors, and neither materially altered the estimated effects of the environmental covariates (Supplementary Section S4). They were not retained in the final model because our objective — wall-to-wall prediction across an entire plantation estate — requires covariates that are available as area-wide rasters, which neither cultivar nor thinning history is.

4.2. Size-dependent composition: apparent recovery and growth suppression

The progressive shift from c3/c4 dominance in the smallest DBH and tree-height classes to c1 dominance in the largest (Fig. 4) reflects the combined action of two processes during stem maturation: apparent recovery of swept stems through eccentric basal growth, and divergent growth rates between swept and straight individuals.

The first process, apparent recovery, arises from eccentric secondary growth in the lower stem. Taira (1987) showed that the asymmetry of basal diameter growth — towards the downslope or upslope side, depending on the orientation of the bend — progressively reduced the visible lean. Tsukahara et al. (1975) reported that stem deviation of approximately 120 cm at age 15 years declined to approximately 70 cm by age 35–40 years. This recovery is driven by diameter increment, so trees with higher growth rates accumulate more compensatory growth in less time and therefore appear straighter at any given age; slow-growing trees retain their visible deformation longer.

The second and arguably more important process is that swept trees grow more slowly than straight ones, both in height and in diameter. Taira (1982, 1985) demonstrated experimentally that saplings prevented from being prostrated by early-winter snow outperformed untreated controls in height, diameter and new-foliage production. Two mechanisms contribute: (i) root damage — particularly mortality of upslope-side roots — during prostration reduces water and nutrient uptake (Sudo et al., 1971; Taira, 1985); and (ii) compression-wood formation during re-erection diverts photosynthates from height extension to basal diameter growth (Taira, 1985). In a pot experiment, Taira (1985) found that the ratio of compression wood to total wood was approximately five times higher in prostrated saplings than in upright controls, with a corresponding reduction in height increment. Sakaue and Taira (1986) subsequently showed, across 16 Japanese cedar stands, that more strongly swept individuals reached the inflection point of the Richards height-growth curve earlier and attained lower asymptotic heights, indicating that basal sweep amplifies — rather than merely reflects — differences in juvenile growth potential. The observed size-dependent shift in stem-form composition therefore arises from the joint operation of these two processes, both of which act in the same direction.

4.3. Predictability of compositional response and the c2 anomaly

The model explained 45.7% of compositional variation in Aitchison space and yielded the highest class-specific accuracy for c1 ($R^2 = 0.619$) and the lowest for c2 ($R^2 = 0.225$). The high predictability of c1 is consistent with our central hypothesis that the abundance of straight stems reflects the broad-scale climatic and productivity gradients that govern the duration of the snow-burial window. The compositional R^2 is correspondingly driven largely by the c1 axis.

The low predictability of c2 has two complementary explanations. First, the PCA showed that c2 varied along an axis (PC2) that was essentially orthogonal to the main climate–productivity contrast captured by PC1. The four covariates used here — all of which characterise broad-scale gradients — primarily explain PC1; the drivers of PC2 lie elsewhere. Taira (1982) identified the decisive event in basal-sweep formation as the early-winter tilt of the stem under partial crown loading, before the tree is fully buried. The trajectory of this initial tilt depends on local micro-topography, ground roughness, snow surface conditions and individual canopy asymmetry—variables that operate at scales finer than the covariates we used. Second, c2 occupies the threshold zone between damaged and undamaged trees: it represents stems in which the sweep was not severe enough to extend above breast height. The abundance of c2 therefore depends on small differences in snow conditions and on inter-annual variability of snow loading, both of which are smoothed away in long-term climate normals. The compositional framework reveals this structural distinction; a univariate measure would conceal it.

4.4. Effect of snow depth and the threshold for straight-stem production

Across all three *ilr* coordinates, mean annual maximum snow depth was the dominant predictor (Fig. 5), consistent with the established understanding that basal sweep in Japanese cedar increases with snow depth (Noomote, 1989; Shidei, 1954; Taira, 1987; Tsukahara et al., 1975). The monotonic decline of c1 and rise of c3 and c4 with snow depth (Fig. 6A) is consistent with Kataoka and Sato (1959), who reported a quadratic relationship between the basal sweep ratio and snow depth, and with Taira (1987), who reported a linear relationship between stem deviation and snow depth.

Two features of the snow-depth response are particularly noteworthy. First, the abundance of c1 declined sharply once snow depth exceeded 0.5 m and reached approximately 10% at 1.8 m, indicating a threshold above which production of straight stems becomes increasingly unlikely. Above approximately 1.8 m, the production of straight-stemmed Japanese cedar appears effectively precluded by the snow regime. Second, the unimodal response of c2 (peaking at 1.0–1.5 m) supports an interpretation of c2 as the transition class between unstressed and severely deformed states: in shallow snow, prostration is rare and most stems remain straight; in deep snow, prostration is severe and stems move to c3 and c4; c2 is correspondingly most abundant at intermediate depths where partial prostration is the modal outcome.

4.5. Effect of site index: the site-productivity escape mechanism

Stem-form composition responded strongly and systematically to site index, with the dominant class shifting from c4 to c3 to c2 to c1 as site index increased (Fig. 6B). Consistent with this strong response, site index ranked second in variable importance after mean annual maximum snow depth in all three *ilr*-coordinate models (Fig. 5), confirming the joint dominance of these two factors anticipated by our hypothesis. This pattern is the predicted outcome of the mechanism that snow-pressure damage depends jointly on snow depth and on the rate at which the sapling escapes the snow-burial window (Noomote, 1992). Trees are at risk of being buried until they exceed approximately 2.0–2.5 times the snow depth (Shidei, 1954); faster height growth, indexed here by site index, shortens this exposure window and reduces cumulative deformation. The result quantifies, at the stand-composition level, a relationship that has been discussed qualitatively in the older literature (Kataoka and Sato, 1959; Taira, 1987) but not previously expressed as a smooth, monotonic function across a large set of stands.

Because site index reflects stand height growth, it could in principle covary with management history, for example if more productive stands were thinned earlier or more often. This is not the case here: thinning frequency was essentially uncorrelated with site index, and although thinning at TAFPC removes trees on the basis of both size and stem form, adding it to the model left the partial dependence on all four environmental covariates virtually unchanged (Supplementary Section S4). The site-index effect documented here therefore reflects growth-mediated escape from the snow-burial window rather than a management artefact.

A different caveat applies, concerning not stand management but the measurement of site index itself. Our site index is computed from the mean tree height in an existing stand and therefore embeds, in addition to inherent site productivity, the cumulative effect of snow-pressure damage on height growth itself (Sakaue and Taira, 1986; Taira, 1985). Stands that have been severely affected by snow pressure will have lower observed tree heights and therefore lower estimated site indices than their inherent productivity would predict. The observed site-index–composition relationship therefore reflects two reinforcing pathways acting in the same direction: (i) high inherent productivity allows early escape from the snow-burial window, increasing c1; and (ii) severe snow-pressure damage suppresses height growth, decreasing the estimated site index of c3- and c4-dominated stands. The composite signal is biologically meaningful for management — it identifies the stands that, in the current climate, deliver high straight-stem yields — but it should not be interpreted as a clean estimate of the marginal effect of site quality at fixed snow loading.

4.6. Slope gradient: two breakpoints and the snow-glide regime

The slope-gradient PDP exhibited two distinct breakpoints, at 15° and 32°, and we interpret these as marking transitions in the snow-loading regime. Between 15° and 32°, the abundance of c1 declined monotonically while c2, c3 and c4 all increased, consistent with the established result that increasing slope amplifies both the downslope component of snow creep and the prostration angle of buried saplings (Taira, 1987).

Above 32°, the pattern qualitatively changed: c4 declined, c1 saturated at low abundance, and c2 increased sharply. We attribute this to the increasing instability of the snowpack on steep slopes. Shidei (1954) noted that on very steep slopes the snowpack is mobile, snow pressure is correspondingly reduced, and the avalanche risk rises. Okamoto et al. (2004) used airborne LiDAR to demonstrate patches of reduced snow depth on steep slopes attributable to localised avalanching. Full-depth avalanches occur with increasing frequency above approximately 30° (Schweizer et al., 2003), and the 32° breakpoint we identify lies in this transition zone. We therefore interpret the response above 32° as reflecting reduced effective snow depth and shorter effective burial duration on the steepest slopes: the most severe deformations (c4) become less common, but the conditions remain unfavourable for production of fully straight stems, so the composition shifts towards the intermediate c2.

4.7. Aspect: insolation-mediated snow persistence

The northness PDP showed a clear asymmetric effect of aspect (Fig. 6D): the abundance of c1 was approximately twice as high on south-facing slopes ($N = -1$) as on north-facing slopes ($N = +1$), and c4 showed the reverse pattern. Slope aspect is well documented to influence snow depth, snow water equivalent and snow duration (Molotch et al., 2005; Okamoto et al., 2004; Saydi and Ding, 2020), and the contrasting responses of c1 and c4 most likely reflect such aspect-driven differences in snow conditions. As Kono (1934) noted, south-facing slopes receive greater insolation and thus undergo earlier snowmelt, which shortens the effective burial period and reduces snow-pressure loading, whereas north-facing slopes retain snow longer and therefore accumulate greater cumulative load. The abundance of c2, by contrast, was essentially insensitive to aspect, consistent with its independence of the dominant climatic gradients.

4.8. Spatial application: elevational dichotomy and east–west gradient

The wall-to-wall application of the model revealed a strongly bimodal spatial structure organised around an elevational threshold near 350 m. Below this elevation, c1 and c2 dominate; above it, c3 and c4 dominate. This elevational dichotomy is the spatial expression of the non-linear, threshold-like responses of stem-form composition to snow depth and site index documented in the PDPs. The local environmental boundary corresponds approximately to a mean annual maximum snow depth of 0.5–1.8 m, broadly demarcating the climate envelope within which straight-stem production becomes viable.

At low elevation, a pronounced east–west gradient emerged: c1 was most abundant in the west ($\sim$38%) and least abundant in the east ($\sim$15%). This gradient reflects the orographic snowfall pattern: the Hida Mountains intercept moist north-westerly air, and the eastern lowlands of Toyama therefore experience higher snow loading than the western lowlands at comparable elevation. At high elevation, no clear east–west gradient was detected: once snow loading exceeds the threshold for severe deformation, additional snow has a diminishing impact on composition, and the regional differences in snow regime are largely masked.

Throughout the study area, the abundance of c2 remained close to 30%, regardless of district or elevation. This is consistent with the interpretation of c2 as a transition class with stochastic, fine-scale determinants, rather than a class whose abundance varies along the dominant climatic gradients.

4.9. Implications for forest management

The model provides a spatially explicit, environmentally grounded prediction of the stand-level composition of stem-form classes across an entire population of plantations. Two applications follow directly. First, combined with the stem-form-class-weighted merchantable-volume equation and product-grade assortment-ratio equations (for sawlogs, plywood logs and chips) of Zushi and Kato (2015) and Zushi et al. (2017), the model permits sequential estimation of stem-form composition, merchantable volume and product-grade-specific volume from environmental covariates alone. This supports broad-scale forecasting of timber supply by product grade. Second, the abundance of c3 and c4 captures the cumulative legacy of snow-pressure damage and provides a quantitative indicator of the value at risk in a stand. The spatial pattern of c3+c4 therefore supports prioritisation of rehabilitation effort (including snow lifting in subsequent rotations) and identification of areas where reforestation may not be economically viable under the current snow regime.

4.10. Implications under a changing climate

Our model uses climatological normals of mean annual maximum snow depth (1981–2010) as a static input, and two temporal issues deserve comment. First, snow depth in this region has not been stationary. A Mann–Kendall analysis of 64 stations in Toyama Prefecture over 1973–2015 found significant decreasing trends in winter snow depth at most low-elevation (plain) stations, whereas mountainous stations showed no significant trend (Oda et al., 2018); a decline in the frequency of heavy-snow years since around 1990 has likewise been reported for the prefecture (Zushi, 2024). The normals we used therefore average over a period of gradual, elevation-dependent decline. This does not undermine the model, because it estimates a spatial relationship — how stem-form composition varies with snow depth across sites — rather than a temporal trend; provided this relationship is stationary, the model remains valid as a spatial prediction tool even as absolute snow depths change. Second, our response variable is inherently cumulative: basal sweep in stands aged 40 years and over integrates snow loading across many juvenile winters, so a long-term average input is appropriate and interannual variability is largely averaged out in the response itself; year-to-year departures that a given cohort experienced are not captured and contribute to the unexplained variance.

Because our model expresses stem-form composition as a function of environmental drivers, it also provides a basis for anticipating how a changing snowfall regime may reshape stem quality. Regional climate ensembles for central Japan project that warming will reduce total winter snowfall along the low-elevation Sea of Japan coast, where snowfall is increasingly converted to rain, while maximum snow depth persists — and heavy daily snowfall may even intensify — in the high-elevation interior, where atmospheric moistening dominates and temperatures remain below freezing (Kawase et al., 2016, 2021). This projected divergence is consistent with the observed elevation-dependent trends noted above and mirrors the elevational contrast in our predicted stem-form composition (Section 4.8), implying that snow-pressure-induced basal sweep may ease in low-elevation stands but persist or worsen in high-elevation ones, rather than declining uniformly. In principle, such projections could be propagated quantitatively through our model: downscaled snow-depth fields from regional climate ensembles could replace the observed normals as input, yielding maps of projected stem-form composition under alternative scenarios. Three challenges attend such an exercise. These projections are typically expressed as snowfall or precipitation rather than the maximum snow depth our model requires, so an intermediate snowpack model would be needed to convert them; their spatial resolution is coarser than our 20 m grid and would require downscaling; and the approach assumes that the fitted snow-depth–stem-form relationship, together with the site-index and topographic effects, remains stationary under a future climate. A partially compensating pathway, not represented in our static formulation, is that warming-driven gains in early height growth would shorten the snow-burial window, all else being equal, reducing deformation at a given snow depth. We therefore regard a full climate-projection exercise as an important next step rather than a result of the present study, and note that the fitted model provides the transfer function such an exercise would require. In this respect, our framework complements the existing mechanistic and statistical models of crown snow damage in northern Europe (Päätalo, 2000; Suvanto et al., 2021), extending the spatial-modelling toolkit to the chronic, snow-pressure-driven deformation that dominates snow damage in oceanic heavy-snow regions.

5. Conclusions

Stand-level stem-form composition in snowy *Cryptomeria japonica* plantations is governed principally by snow depth and site productivity, and their effects are strongly non-linear. Straight-stem production declines sharply once mean annual maximum snow depth exceeds about 0.5 m and is effectively precluded above about 1.8 m, whereas higher site productivity offsets this loss by shortening the snow-burial window.

Slope modifies these effects through two breakpoints, at 15° and 32°, the latter marking the onset of snow glide and avalanching. Mapped across an entire plantation estate, these relationships produce a sharp elevational dichotomy near 350 m, above which severely swept stems dominate. This framework provides, to our knowledge, the first wall-to-wall spatial prediction of snow-pressure damage, and a practical basis for product-grade-aware supply forecasting, reforestation siting and adaptation planning in oceanic heavy-snow forests.

CRediT authorship contribution statement

Kotaro Zushi: Writing – review & editing, Writing – original draft, Visualization, Software, Methodology, Formal analysis, Data curation, Conceptualization. **Akio Kato:** Writing – review & editing, Investigation. **Hisashi Sugita:** Writing – review & editing, Investigation.

Declaration of Generative AI and AI-assisted technologies in the writing process

During the preparation of this work, the authors used Claude (Anthropic) to translate an initial draft written in Japanese into English and to improve the language and readability of the English text. After using this tool, the authors reviewed and edited the content as needed and take full responsibility for the content of the published article. The tool was not used for study design, data collection, data analysis, interpretation of results or the selection and generation of references, all of which were carried out by the authors.

Funding

This research did not receive any specific grant from funding agencies in the public, commercial, or not-for-profit sectors.

Declaration of competing interest

The authors declare that they have no known competing financial interests or personal relationships that could have appeared to influence the work reported in this paper.

Acknowledgements

We thank the Toyama Prefectural Agriculture, Forestry and Fisheries Public Corporation for access to plantations and inventory records, and the staff of the Forest Research Institute, Toyama Prefectural Agricultural, Forestry and Fisheries Research Center, for field assistance.

Appendix A. Supplementary data

Supplementary material related to this article can be found online at https://doi.org/10.1016/j.foreco.2026.124172.

Data availability

The data that support the findings of this study were provided by the Toyama Prefectural Agriculture, Forestry and Fisheries Public Corporation. Restrictions apply to the availability of these data, which were used under licence for this study. Data are available from the authors with the permission of the Toyama Prefectural Agriculture, Forestry and Fisheries Public Corporation.

References

Aitchison, J., 1982. The statistical analysis of compositional data. J. R. Stat. Soc. Ser. B Stat. Methodol. 44, 139–160.

Aiura, H., Nakajima, H., Ishida, M., 2018. Estimate average annual maximum snow depth with the temperature and the amount of precipitation of the mesh normal climatic data in Toyama Prefecture, Japan. J. Jpn. For. Soc. 100, 174–177, In Japanese with English abstract.

Biecek, P., 2018. DALEX: Explainers for complex predictive models in R. J. Mach. Learn. Res. 19, 1–5, URL: https://jmlr.org/papers/v19/18-416.html.

Biecek, P., Baniecki, H., 2023. Ingredients: Effects and importances of model ingredients. URL: https://CRAN.R-project.org/package=ingredients. R package version 2.3.0.

Egozcue, J.J., Pawlowsky-Glahn, V., Mateu-Figueras, G., Barcelo-Vidal, C., 2003. Isometric logratio transformations for compositional data analysis. Math. Geol. 35, 279–300.

Frutiger, H., Kuster, J., 1967. Über das gleiten und kriechen der schneedecke in Lawinenverbauungen. Schweiz. Z. Für Forstwes. 118, 633–643.

In der Gand, H., 1968. Aufforstungsversuche an einem Gleitschneehang. Mitteilungen der Schweiz. Anst. Für Das Forstl. Vers. 44, 233–326, URL: https://www.dora.lib4ri.ch/wsl/islandora/object/wsl:13418/datastream/PDF/in_der_Gand-1968-Aufforstungsversuche_an_einem_Gleitschneehang._Ergebnisse-(published_version).pdf.

Gardiner, B., Peltola, H., Kellomäki, S., 2000. Comparison of two models for predicting the critical wind speeds required to damage coniferous trees. Ecol. Model. 129, 1–23.

Hada, S., 1960. Studies on the utilizing volume (5): On the volume of butt-sweep. J. Jpn. For. Soc. 42, 127–135, In Japanese with English abstract.

Höller, P., Fromm, R., Leitinger, G., 2009. Snow forces on forest plants due to creep and glide. Forest Ecol. Manag. 257, 546–552. http://dx.doi.org/10.1016/j.foreco.2008.09.035.

Imanaga, M., Kitamura, M., Hosaka, Y., 1979. Stand establishment results of sugi (*Cryptomeria japonica*) plantations around Mt. Gassan. In: Comprehensive Study on Forest Management in Heavy Snowfall Areas: Research Report. Faculty of Agriculture, Yamagata University, In Japanese.

Kataoka, K., Sato, S., 1959. On the bend of lower part of the afforested cryptomeria by snow. Seppyo (J. Soc. Snow Ice) 21, 13–19, In Japanese with English abstract.

Kato, A., Tanaka, K., 2009. The Growth Parameters of the System Yield Table 'Silv-No-Mori' in Tateyama-Sugi (*Cryptomeria Japonica* D. Don) Stands. Research Report, Toyama Prefectural Research Center for Forestry and Fisheries, Forest Research Institute, pp. 44–51, In Japanese with English abstract.

Kawase, H., Murata, A., Mizuta, R., Sasaki, H., Nosaka, M., Ishii, M., Takayabu, I., 2016. Enhancement of heavy daily snowfall in central Japan due to global warming as projected by large ensemble of regional climate simulations. Clim. Change 139, 265–278.

Kawase, H., Murata, A., Yamada, K., Nakaegawa, T., Ito, R., Mizuta, R., Nosaka, M., Watanabe, S., Sasaki, H., 2021. Regional characteristics of future changes in snowfall in Japan under RCP2.6 and RCP8.5 scenarios. SOLA 17, 1–7.

Kono, J., 1934. Snow damage and growth conditions of afforested trees in heavy snowfall regions. J. Jpn. For. Soc. 16, 1006–1016, In Japanese.

Kuhn, M., Wickham, H., 2020. Tidymodels: a collection of packages for modeling and machine learning using tidyverse principles. URL: https://www.tidymodels.org.

Leaphart, C.D., Hungerford, R.D., Johnson, H.E., 1972. Stem Deformities in Young Trees Caused by Snowpack and Its Movement. Research Note INT-158, USDA Forest Service, Intermountain Forest and Range Experiment Station, Ogden, Utah.

Leitinger, G., Höller, P., Tasser, E., Walde, J., Tappeiner, U., 2008. Development and validation of a spatial snow-glide model. Ecol. Model. 211, 363–374. http://dx.doi.org/10.1016/j.ecolmodel.2007.09.025.

Martín-Fernández, J.A., Barceló-Vidal, C., Pawlowsky-Glahn, V., 2003. Dealing with zeros and missing values in compositional data sets using nonparametric imputation. Math. Geol. 35, 253–278.

Ministry of Land, Infrastructure, Transport and Tourism (MLIT), 2026. National land numerical information: Meteorological observation points (g02), version 3.0. https://nlftp.mlit.go.jp/ksj/gml/datalist/KsjTmplt-G02-v3_0.html. (Accessed 10 February 2026); in Japanese.

Molotch, N.P., Colee, M.T., Bales, R.C., Dozier, J., 2005. Estimating the spatial distribution of snow water equivalent in an alpine basin using binary regression tree models: the impact of digital elevation data and independent variable selection. Hydrol. Process. 19, 1459–1479.

Noomote, M., 1984. Silvicultural techniques in heavy snowfall areas (VII): Methods and effects of righting snow-bent trees. Bull. the Niigata Prefect. For. Exp. Stn. 26, 31–41, In Japanese.

Noomote, M., 1989. Snow Damage and Silvicultural Techniques for Sugi (*Cryptomeria Japonica*) Plantations in Wet Heavy Snowfall Areas. Niigata Prefectural Forest Experiment Station, Niigata, Japan, In Japanese.

Noomote, M., 1992. Rate of successful afforestation and number of snow burial in sugi plantations in the heavy snowfall region. Seppyo (J. Soc. Snow Ice) 54, 159–164, In Japanese.

Nykänen, M.L., Broadgate, M., Kellomäki, S., Peltola, H., Quine, C., 1997. Factors affecting snow damage of trees with particular reference to European conditions. Silva Fenn. 31.

Oda, S., Matsuura, T., Shimosaka, M., Tebakari, T., 2018. Long-term changes in snowfall and snow depth in Toyama prefecture during 1974–2015. J. Jpn. Soc. Civ. Eng. Ser. B1 (Hydraulic Engineering) 74, I_73–I_78, (In Japanese with English abstract).

Okamoto, T., Kurokawa, U., Matsuura, J., Asano, S., Matsuyama, K., 2004. Adaptability of an airborne laser scanner to determine a snow depth distribution on a mountain area. J. Jpn. Soc. Hydrol. Water Resour. 17, 529–535, In Japanese with English abstract.

Päätalo, M.L., 2000. Risk of snow damage in unmanaged and managed stands of scots pine, Norway spruce and birch. Scand. J. For. Res. 15, 530–541.

Peltola, H., Kellomäki, S., 1993. A mechanistic model for calculating windthrow and stem breakage of scots pines at stand edge. Silva Fenn. 27, 99–111. http://dx.doi.org/10.14214/sf.a15679.

Peltola, H., Kellomäki, S., Hassinen, A., Granander, M., 2000. Mechanical stability of scots pine, Norway spruce and birch: an analysis of tree-pulling experiments in Finland. Forest Ecol. Manag. 135, 143–153.

Peltola, H., Kellomäki, S., Väisänen, H., Ikonen, V.P., 1999. A mechanistic model for assessing the risk of wind and snow damage to single trees and stands of scots pine, Norway spruce, and birch. Can. J. Forest Res. 29, 647–661.

Peltola, H., Nykänen, M.L., Kellomäki, S., 1997. Model computations on the critical combination of snow loading and windspeed for snow damage of scots pine, Norway spruce and birch sp. at stand edge. Forest Ecol. Manag. 95, 229–241. http://dx.doi.org/10.1016/S0378-1127(97)00037-6, URL: https://www.sciencedirect.com/science/article/pii/S0378112797000376.

Petty, J., Worrell, R., 1981. Stability of coniferous tree stems in relation to damage by snow. For.: An Int. J. For. Res. 54, 115–128.

R Core Team, 2024. R: A Language and Environment for Statistical Computing. R Foundation for Statistical Computing, Vienna, Austria, URL: https://www.R-project.org/.

SAGA GIS Development Team, 2020. SAGA GIS (system for automated geoscientific analyses), version 7.8.2. http://www.saga-gis.org. (Accessed 24 February 2026).

Sakaue, T., Taira, H., 1986. Height growth pattern of Tateyama-sugi (*Cryptomeria japonica* D. Don) (II): Influence of basal bending on height growth. J. Jpn. For. Soc. 11, 24–32, In Japanese with English abstract.

Saydi, M., Ding, J.l., 2020. Impacts of topographic factors on regional snow cover characteristics. Water Sci. Eng. 13, 171–180.

Schmidt, W.C., Schmidt, J.A., 1979. Recovery of Snow-Bent Young Western Larch. General Technical Report INT-54, USDA Forest Service, Intermountain Forest and Range Experiment Station, Ogden, Utah.

Schweizer, J., Jamieson, J.B., Schneebeli, M., 2003. Snow avalanche formation. Rev. Geophys. 41, 1016. http://dx.doi.org/10.1029/2002RG000123.

Shidei, T., 1954. Studies on the damage to forest trees caused by snow pressure. Bull. For. For. Prod. Res. Inst. 1–89, In Japanese with English abstract.

Sudo, S., Tsukahara, H., Kitamura, M., 1971. Changes in lateral root position of young sugi (*Cryptomeria japonica*) trees on steep slopes with heavy snowfall. In: Proceedings of the 82nd Annual Meeting of the Japanese Forestry Society. pp. 195–196, In Japanese.

Suvanto, S., Lehtonen, A., Nevalainen, S., Lehtonen, I., Viiri, H., Strandström, M., Peltoniemi, M., 2021. Mapping the probability of forest snow disturbances in Finland. PLoS One 16, 1–20. http://dx.doi.org/10.1371/journal.pone.0254876, URL: https://doi.org/10.1371/journal.pone.0254876.

Taira, H., 1979. Sugi clonal varieties in Toyama Prefecture. Bull. the Toyama Prefect. For. Exp. Stn. 5, Toyama Prefectural Forest Experiment Station. In Japanese with English abstract.

Taira, H., 1982. The influence of differences in the damage of initial snow throw effected by early winter snow on basal bending in young sugi (*Cryptomeria japonica* d. don). J. Jpn. For. Soc. 64, 453–460, In Japanese with English abstract.

Taira, H., 1984. Snow pressure damage resistance of sugi (*Cryptomeria japonica*) clonal varieties in heavy snowfall areas. Bull. the Toyama Prefect. For. Exp. Stn. 10, 24–29, In Japanese with English abstract.

Taira, H., 1985. Basal-bend formation in young sugi (*Cryptomeria japonica*). J. Jpn. For. Soc. 67, 11–19, In Japanese with English abstract.

Taira, H., 1987. The study of mechanism of sugi basal bending and its control methods. Bull. the Toyama Prefect. For. Exp. Stn. 1–81, In Japanese with English abstract.

Taira, H., 1991. Snow-cover condition in Japan and damage of the sugi (*Cryptomeria japonica* d. don). In: Proceedings of the IUFRO Technical Session on Geomorphic Hazards in Managed Forests. General Technical Report PSW-GTR-130, USDA Forest Service, pp. 65–71, Raymond M. Rice (Technical Coordinator).

Tomppo, E., Antropov, O., Praks, J., 2019. Boreal forest snow damage mapping using multi-temporal Sentinel-1 data. Remote. Sens. 11, 384.

Tsukahara, H., Otani, H., Sudo, S., 1975. The bending of root sides of the forest trees planted by *Cryptomeria* seedlings on the steep stands in a heavy snowy region. J. the Yamagata Agric. For. Soc. 32, 21–30, In Japanese.

van den Boogaart, K.G., Tolosana-Delgado, R., Bren, M., 2025. Compositions: Compositional data analysis. URL: https://CRAN.R-project.org/package=compositions. R package version 2.0-9.

Venäläinen, A., Lehtonen, I., Laapas, M., Ruosteenoja, K., Tikkanen, O.P., Viiri, H., Ikonen, V.P., Peltola, H., 2020. Climate change induces multiple risks to boreal forests and forestry in Finland: A literature review. Global Change Biol. 26, 4178–4196. http://dx.doi.org/10.1111/gcb.15183, URL: https://onlinelibrary.wiley.com/doi/abs/10.1111/gcb.15183, arXiv:https://onlinelibrary.wiley.com/doi/pdf/10.1111/gcb.15183.

Wright, M.N., Ziegler, A., 2017. ranger: A fast implementation of random forests for high dimensional data in C++ and R. J. Stat. Softw. 77, 1–17. http://dx.doi.org/10.18637/jss.v077.i01.

Yano, S., 1987. Studies on prevention of snow damage in plantations in Hyogo prefecture (II): Survey on the health condition of plantations. Bull. the Hyogo Prefect. For. Exp. Stn. 33, 1–14, In Japanese.

Zimovà, S., Dobor, L., Hlásný, T., Rammer, W., Seidl, R., 2020. Reducing rotation age to address increasing disturbances in Central Europe: Potential and limitations. Forest Ecol. Manag. 475, 118408. http://dx.doi.org/10.1016/j.foreco.2020.118408, URL: https://www.sciencedirect.com/science/article/pii/S0378112720311774.

Zushi, K., 2024. Spatial estimation of the operational quantity to prevent bending due to snow pressure in Toyama, Japan. Bull. the Toyama Prefect. Agric. For. Fish. Res. Cent. For. Res. Inst. 16, 7–17, In Japanese with English abstract.

Zushi, K., Kato, A., 2015. Estimation of merchantable volume and volume ratio by log grade in sugi (*Cryptomeria japonica*) crooked trees using stem crookedness class. J. Jpn. For. Soc. 97, 269–275. http://dx.doi.org/10.4005/jjfs.97.269, In Japanese with English abstract.

Zushi, K., Kato, A., Aiura, H., 2017. The effect of bucking methods in crooked sugi (*Cryptomeria japonica*) trees on the production of low-quality logs for biomass power generation. J. Jpn. For. Soc. 99, 259–265. http://dx.doi.org/10.4005/jjfs.99.259, In Japanese with English abstract.